Highly Active Anode Electrocatalysts Derived from Electrochemical Leaching of Ru from Metallic $Ir_{0.7}Ru_{0.3}$ for Proton Exchange Membrane Electrolyzers

Li Wang[a], Viktoriia A. Saveleva[b], Spyridon Zafeiratos[b], Elena R. Savinova[b], Philipp Lettenmeier[a], Pawel Gazdzicki[a], Aldo S. Gago[a,*], K. Andreas Friedrich[a,c]

[a]Institute of Engineering Thermodynamics, German Aerospace Center (DLR), Pfaffenwaldring 38-40, 70569 Stuttgart, Germany

[b]Institut de Chimie et Procédés pour l'Energie, l'Environnement et la Santé, UMR 7515 du CNRS-UdS 25 Rue Becquerel, 67087 Strasbourg, France

[c]Institute of Energy Storage, University of Stuttgart, Pfaffenwaldring 31, 70569 Stuttgart, Germany

KEYWORDS: OER catalyst; Mixed oxide; Ru leaching; Activity; Stability; PEM electrolyzer

Abstract

Hydrogen produced by water splitting is a promising solution for a sustained economy from renewable energy sources. Proton exchange membrane (PEM) electrolysis is the utmost suitable technology for this purpose, although the quest for low cost, highly active and durable catalysts is persistent. Here we develop a nanostructured iridium catalyst after electrochemically leaching ruthenium from metallic iridium-ruthenium, $Ir_{0.7}Ru_{0.3}O_x$ (EC), and compare its physical and electrochemical properties to the thermally treated counterpart: $Ir_{0.7}Ru_{0.3}O_2$ (TT). $Ir_{0.7}Ru_{0.3}O_x$ (EC) shows an unparalleled 13-fold higher oxygen evolution reaction (OER) activity compared to the $Ir_{0.7}Ru_{0.3}O_2$ (TT). PEM electrolyzer tests at 1 A cm^{-2} show no increase of cell voltage for almost 400 h, proving that $Ir_{0.7}Ru_{0.3}O_x$ (EC) is one of the most efficient anodes so far developed.

* Corresponding author: Tel.: +49 711 6862-8090, fax: +49 711 6862-747, e-mail address: aldo.gago@dlr.de (Aldo S. Gago).

Introduction

Substantial effort has been dedicated for scaling up renewable energy production capabilities to address the climate issues related to environmental pollution. However, large-scale energy storage for balancing the intermittent electricity generated by wind turbines and solar panels is still a challenge. Hydrogen generation by proton exchange membrane (PEM) water electrolysis, is recently considered as a feasible technology to solve this problem thanks to its rapid response, compact design and wide range operation [1,2]. However, high amount of scarce and expensive Ir is needed to catalyze the oxygen evolution reaction (OER), hindering the widespread commercialization of the PEM technology. Moreover, the OER reaction mostly dominates the entire energy losses due to its sluggish kinetics [3,4]. Nevertheless, up to now, the exceptional OER properties of Ir- or IrRu- surface have not been fully understood due to its complexity [5].

Iridium oxide (IrO_2), iridium ruthenium oxide ($IrRuO_2$) or the mixture of Ir and Ru oxides (IrO_2-RuO_2) have been considered for decades as the state-of-the-art OER catalysts in acid electrolyte due to their superior catalytic activity and considerable stability [6–11]. Kötz *et al.* reported that the stability of RuO_2 was significantly improved by admixture of IrO_2, even small amounts (ca. 20%) could dramatically reduce the corrosion rate of RuO_2. A hypothesis based on the electronic band mixing and shift in oxidation potentials was proposed to explain the stabilization mechanism [12]. It was suggested that the electrons available on IrO_2 sites are simultaneously shared with RuO_2 sites, thus preventing Ru from being oxidized to RuO_4, which was identified as the main corrosion product of Ru during the O_2 evolution in acidic media [12,13].

In recent years, highly active electrochemically oxidized OER catalysts have been explored [10,14,15]. Markovic and coworkers reported an inverse relationship between activity and

stability through investigating monometallic and bimetallic Ir- and Ru- oxides [16,17]. Specifically, electrochemically oxidized IrO_x and RuO_x always showed higher activity than the thermally treated IrO_2 and RuO_2, but less stability. The same phenomenon was observed by Kim *et al.* on RuO_x deposited on a Ti substrate [18]. Cherevko *et al.* compared the metallic Ir and IrO_x deposited on a Ti substrate treated under different temperatures from 250 °C to 550 °C. Metallic Ir showed the highest dissolution rate but not the highest OER activity [19]. The IrRu oxide developed by employing Ir surface segregation showed a four-times improved stability while keeping the same activity as the best commercial Ru-Ir alloy anode catalysts. It was attributed to the formation of a nano-segregated Ir-domain that balance the stability and activity of surface atoms [17]. Even though the large amount of efforts on investigating IrO_2-RuO_2 systems since 1980s, there are no reports so far on electrochemical properties of nanostructured metallic Ir-Ru and the effect of leaching Ru from this system. In this context, Seitz *et al.* have recently developed a highly active and stable $IrO_x/SrIrO_3$ OER catalyst by strontium leaching from $SrIrO_3$ thin film [20].

In this study, we report a novel electrochemically oxidized electrocatalyst derived from Ru leaching in $Ir_{0.7}Ru_{0.3}$ metal nanoparticles, $Ir_{0.7}Ru_{0.3}O_x$ (EC), for PEM electrolyzers, which shows superior activity and increased cell efficiency during ca. 400 h electrolyzer stack operation. The dissolution of unstable Ru led to an unparalleled OER activity of the remaining Ir-rich electrocatalyst compared to the classic thermally treated $Ir_{0.7}Ru_{0.3}O_2$ (TT). The enrichment with Ir was confirmed by ultra-high vacuum X-ray photoelectron spectroscopy (UHV-XPS), transmission electron microscopy (TEM) and energy-dispersive X-ray spectroscopy (EDS) on post-mortem membrane electrode assemblies (MEAs). By applying Near-Ambient Pressure X-ray Photoelectron Spectroscopy (NAP-XPS) we show that during the OER Ru in $Ir_{0.7}Ru_{0.3}O_x$

(EC) transforms into unstable $Ru(OH)_x$, which is prone to leaching, contrary to the thermally treated $Ir_{0.7}Ru_{0.3}O_2$ (TT), where Ir stabilizes Ru in a rutile RuO_2 oxide [21].

Results and discussions

Pristine $Ir_{0.7}Ru_{0.3}$ nano-particles ($Ir_{0.7}Ru_{0.3}$–pristine) were prepared by direct reduction of Ir and Ru salts under the protection of capping agent in water-free environment (for details see SI). Electrochemically oxidized state, $Ir_{0.7}Ru_{0.3}O_x$ (EC), was achieved either by potential cycling in the case of RDE measurements in liquid electrolyte or by holding potential at 1.4 V for 1 h in the case of PEM-electrolysis. Previously reported typical thermal treatment protocol [9,22,23], 490 °C in air for 30 min, was applied to obtain $Ir_{0.7}Ru_{0.3}O_2$ (TT), in order to compare with the state-of-the-art OER catalysts.

Physical characterization of catalyst powders

Figure 1 (a, c) shows the TEM and scanning TEM (STEM) images of $Ir_{0.7}Ru_{0.3}$-pristine. A uniform particle dispersion was observed with a mean particle size of ca. 1.5 nm. EDS analysis (Figure S2, see SI) revealed an irregular Ru fraction throughout the sample, between 5 wt.% and 50 wt.%, which indicates that Ir and Ru atoms are non-uniformly distributed on the nano-scale before either EC or TT process. The inhomogeneity of the Ir/Ru distribution was further confirmed by STEM. For example, the STEM image of Figure 1c only comprises Ir particles, with ca. 2 nm particle size. Carbon and $IrCl_3$ impurities arising from residual surfactant and precursor were also observed in as-prepared $Ir_{0.7}Ru_{0.3}O_x$ (EC) sample (Figure S2, see SI). TEM and EDS performed after the EC oxidation under 1.4 V for 1 h (Figure S2 (b), see SI) show partial oxidation of metal nanoparticles accompanied by the particle size growth (up to ca. 3.9 nm). On the other hand, Ir/Ru ratio became more uniform with Ru fraction between 0.2 and 0.4

and impurities (C and $IrCl_3$) disappeared. The corresponding TEM and STEM images of $Ir_{0.7}Ru_{0.3}O_2$ (TT) are shown in Figure 1 (b, d), where larger particles ranging from 3 nm to 9 nm can be observed. By analyzing the live Fast Fourier Transformation (FFT) based on STEM image, the distances between the crystallographic planes have been determined, 2.577 Å and 3.131 Å respectively, further been discerned as (101) and (110) lattice plane distance of a rutile phase, which we attribute to a phase of mixed IrRu dioxide considering the results of the EDS analysis on the homogeneous Ir and Ru distribution. It implies that the as-prepared powder was well crystallized and its atom composition became homogeneous on the nano-scale after the thermal treatment process [21].

Figure S3 (a) shows the XRD spectrum of $Ir_{0.7}Ru_{0.3}$-pristine. Broad diffraction peaks imply a catalyst particle size at the nano-scale, similar as the IrO_x-Ir catalyst reported previously [15]. In addition, chloride impurities were detected in agreement with XPS (Figure S5). The spectrum of $Ir_{0.7}Ru_{0.3}O_2$ (TT) is shown in Figure S3 (b). The sharp diffraction peaks provide evidence for the formation of a rutile $Ir(Ru)O_2$, while neither $IrCl_3$ nor $RuCl_3$ impurities were observed after 490 ^oC annealing for half an hour in air, again in agreement with XPS analysis.

The results of XPS measurements for $Ir_{0.7}Ru_{0.3}$-pristine and subjected to Ar^+ sputtering are depicted in Figure S4 and S5 (supporting information). According to the XPS depth profile analysis thin IrO_2 and RuO_2 surface layers are observed which encapsulate a core consisting of metallic Ir and Ru in the pristine powder. This is also confirmed by the atomic concentration of oxygen, which sharply decreased after 10 s Ar^+ sputtering. Moreover, for the pristine sample no element (neither Ir nor Ru) segregation was observed, yielding a constant atomic ratio Ir/Ru of 2, close to the value of the stoichiometric ratio. Insignificant surface enrichment was found previously in the oxide prepared by reactive sputtering without any further thermal treatment

[24]. XPS data including depth profiling for the $Ir_{0.7}Ru_{0.3}O_2$ (TT) suggest high oxygen concentration in the sample, confirming complete transformation of metallic Ru and most of Ir in respective oxides during the thermal treatment. The observed sift of the Ir4f peaks to lower binding energies during the Ar^+ sputtering (Figure S5) is indicative of the presence of some metal Ir in the particle cores. Note however that Ar^+ sputtering itself may induce oxide decomposition. In addition, a strong Ir surface segregation was observed during the Ar^+ spurring according to the component depth profile analysis with an atomic Ir/Ru surface ratio up to 4.5 (Figure S5, see SI). A similar phenomenon was also reported in the literature when the catalysts were prepared by thermal deposition and afterwards annealed in the temperature range of 400-450 °C for 1-3 hours [24–27].

RDE measurements

Both $Ir_{0.7}Ru_{0.3}O_x$ (EC) and $Ir_{0.7}Ru_{0.3}O_2$ (TT) were characterized by rotating disc electrode (RDE), 10 cycles of cyclic voltammetry (CV) between 0 and 1.6 V vs. RHE were used as EC protocol (Figure S7, see SI) for both catalysts, 1.6 V was applied as upper potential limit based on two considerations: i) strong oxygen evolution and Ru dissolution have already occurred up to this potential [17,28] and ii) higher potential could lead to a GC-RDE damage due to the carbon oxidation. Mass activity changes between EC and TT are shown in Figure S7 (see SI). It is observed that after a few potential cycles up to 1.6 V the $Ir_{0.7}Ru_{0.3}O_x$ (EC) sample was stabilized (apparently by leaching significant proportion of Ru out of the catalysts as confirmed by TEM, EDS and ex situ XPS) and reached a steady state showing an insignificant mass activity change during subsequent operation. Post-EC protocol (figure S7, see SI) was carried out to confirm the stabilized particle surface of $Ir_{0.7}Ru_{0.3}O_x$ (EC), OER activity and CVs were recorded for comparison. From figure S7 (see SI), stable mass OER activities after post-EC protocol and

overlapped CVs on different cycles strongly imply that both EC and TT sample have a stable particle surface. The $Ir_{0.7}Ru_{0.3}O_x$ (EC) was apparently. Therefore, 2nd cycles after the EC-protocol were selected for the OER mass activity comparison and the results are shown in Figure 2 (a) for samples $Ir_{0.7}Ru_{0.3}O_x$ (EC), $Ir_{0.7}Ru_{0.3}O_2$ (TT) and IrO_x (EC), which is our previously published catalyst with superior activity [15]. Among these 3 catalysts, $Ir_{0.7}Ru_{0.3}O_x$ (EC) showed the best OER performance, much higher than $Ir_{0.7}Ru_{0.3}O_2$ (TT), while IrO_x (EC) is in the position between $Ir_{0.7}Ru_{0.3}O_x$ (EC) and $Ir_{0.7}Ru_{0.3}O_2$ (TT). After stabilization, Tafel plots of $Ir_{0.7}Ru_{0.3}O_x$ (EC) and $Ir_{0.7}Ru_{0.3}O_2$ (TT) are 39.7 mV dec^{-1} and 60.4 mV dec^{-1} respectively, show in insets of Figure 2(a), thus demonstrating the superior electrocatalytic activity of $Ir_{0.7}Ru_{0.3}O_x$ (EC) relative to the $Ir_{0.7}Ru_{0.3}O_2$ (TT). Figure 2(b) compares the mass activity of EC and TT samples for an overpotential of 250 mV. $Ir_{0.7}Ru_{0.3}O_x$ (EC) shows ca. 13 times higher activity than $Ir_{0.7}Ru_{0.3}O_2$ (TT), while still 6 times higher than IrO_x (EC), our benchmark catalyst. Moreover, $Ir_{0.7}Ru_{0.3}O_x$ (EC) showed lower overpotentials under current densities of either 0.1 mA cm^{-2} or 5 mA cm^{-2} than $Ir_{0.7}Ru_{0.3}O_2$ (TT), 195.5 mV and 268.7 mV respectively, while 238 mV and 336 mV respectively for $Ir_{0.7}Ru_{0.3}O_2$ (TT) in the same condition (Figure S9, see SI). The difference between overpotentials of $Ir_{0.7}Ru_{0.3}O_x$ (EC) and $Ir_{0.7}Ru_{0.3}O_2$ (TT) increased with the current density, even though they showed similar onset potentials of 1.398 V and 1.410 V vs. RHE, respectively (Figure S10, see SI). In addition, RuO_x (EC) was also added in figure 2(a) for comparison, it shows the lowest overpotential for catalyzing OER, but is rather unstable with an activity peak at 1.491 V vs. RHE, which apparently results from Ru corrosion [28]. The activity peak position is slightly lower than the one reported by Reier *et al.* [29]. For higher potentials this catalyst cannot compete with Ir-based electrocatalysts due to its decreasing activity. For tracking the changes of the catalyst surface, CVs during the EC-protocol on both $Ir_{0.7}Ru_{0.3}O_x$ (EC)

and $Ir_{0.7}Ru_{0.3}O_2$ (TT) were recorded and are shown in Figure 2 (c) and (d) respectively. While for the $Ir_{0.7}Ru_{0.3}O_2$ (TT) sample scans 2 and 10 coincide suggesting stability of the surface against Ru dissolution during the electrochemical protocol, significant differences were observed between scan 2 and scan 10 of the $Ir_{0.7}Ru_{0.3}O_x$ (EC) below 0.3 vs. RHE demonstrating surface changes. The cathodic peak, which has been attributed in the literature either to the atomic hydrogen absorption into the catalyst lattice and grain boundaries [8,30], or to hydrogen evolution on RuO_2 [31], almost disappeared after the EC protocol in scan 10, indicating that: i) Ru was leached out from the surface of $Ir_{0.7}Ru_{0.3}O_x$ (EC) sample into electrolyte solution; ii) surface metallic Ir phase was oxidized to IrO_x. Due to the low Ru/Ir ratio in the $Ir_{0.7}Ru_{0.3}O_x$ (EC) catalyst and surface IrO_x formation, a suppression of the hydrogen absorption and evolution can be expected [8]. In addition, the $Ir_{0.7}Ru_{0.3}O_x$ (EC) sample exhibits an apparent larger capacitance than the TT, which in general reflects the electrode capacity for charge accumulation at the electrode/electrolyte interface [8]. This difference can be explained by the particle size difference between the EC and TT, leading to a higher electrode/electrolyte interface in the case of $Ir_{0.7}Ru_{0.3}O_x$ (EC).

XPS analysis of electrode samples

In order to investigate the long term stability of Ru components under water electrolysis conditions, membrane electrode assemblies (MEAs) were prepared by using both materials, $Ir_{0.7}Ru_{0.3}O_x$ EC and TT, as anode catalysts, followed by an electrochemical activation for 1 h at 1.4V and operation of 18 h at 1.6 V, which is in line with the upper potential limit of RDE measurements to simplify comparison. Post mortem analysis by using TEM and UHV-XPS were carried out afterwards and compared with the as-prepared electrodes. EDS analysis coupled with TEM in Figure S13 (see SI) indicates drop of the Ru contribution below the detection limit of ca.

10% after 18 h water electrolysis at 1.6V in the $Ir_{0.7}Ru_{0.3}O_x$ (EC) electrode while the $Ir_{0.7}Ru_{0.3}O_2$ (TT) electrode showed a similar Ir/Ru ratio before and after operation. This outcome is in agreement with the XPS depth profiles depicted in Figure 3. While in the EC sample before operation the Ir/Ru ratio is around 2, after 18h at 1.6 V it increases up to 8 for >50s sputtering (see Figure 3a), i.e. a leaching of approximately 85% of Ru upon operation of the EC sample is unambiguously observed. The decreased Ir/Ru ratio for sputter times <50s indicates a slightly increased Ru concentration at the surface compared to bulk due to the segregation process.

In the case of the TT sample (Figure 3b) the Ir/Ru ratios are similar before and after operation. While in the as-prepared sample an increased Ir surface concentration is observed, the sample after operation is even more homogeneous with an almost constant Ir/Ru ratio of 2-3.

The depth profiles in Figure 3(c) and (d) show the Ir-oxide percentage in the entire amount of the Ir signal before and after electrolysis operation of the EC and TT samples, respectively. Apparently, the percentage of Ir-oxide does not change in the EC sample after operation. In both cases, an oxide dominated surface layer is observed. After sputtering times >100s the oxide fraction decreases below 10%.

In the TT sample the fraction of Ir-oxide is substantially higher than in the EC sample and, for long sputter times, increases from 20% to 30% after operation. Moreover, the surface Ir-oxide dominated layer is much thicker in the EC sample than in the TT material. Specifically, 10 times longer sputter times are needed for the TT sample compared to the EC sample to reduce the Ir-oxide fraction to values <50%.

These results are evidence that RuO_2 in the $Ir_{0.7}Ru_{0.3}O_2$ (TT) is significantly stable than in the EC sample since it is stabilized by the presence of IrO_2. It implies that the oxide form of Ir is very

crucial for the Ru stabilization as recently reported [21]. Less IrO_x in the EC sample leads to the fast Ru dissolution. NAP-XPS in operando measurements (See SI) suggest that until the $Ir_{0.7}Ru_{0.3}O_x$ (EC) sample is stabilized, Ru under the OER conditions is transformed into an unstable Ru(IV) hydroxide, which is prone to dissolution. The situation is different for the $Ir_{0.7}Ru_{0.3}O_2$ (TT), where Ir oxide stabilizes Ru in the form of rutile RuO_2, which is much more resistant against corrosion. Note also that RuO_4, which we consider as the OER intermediate [21], was detected on the surface of both EC and TT samples, being stabilized in the latter by the interaction with the underlying $Ru(Ir)O_2$.

Electrolyzer measurements

Figure 4 (a) depicts the electrochemical characterization of the 2-cell stack by employing $Ir_{0.7}Ru_{0.3}O_x$ (EC) and $Ir_{0.7}Ru_{0.3}O_2$ (TT) as anodes respectively. It demonstrated the cell performance difference after one day activation running at 80 °C. As we can see, the cell with TT anode shows apparently higher potential, up to 45 mV at maximum, relative to the one using EC under the same current density. In order to confirm the contribution of $Ir_{0.7}Ru_{0.3}O_x$ (EC) for the improved cell performance, electrochemical impedance spectroscopy (EIS) was performed to exclude possible falsifications due to assembling, ohmic resistances and mass transport limitations, and the results are shown in Figure S14 (see SI). Analyzing the EIS results by using an equivalent circuit shown in Figure S14, which consists of one ohmic and three R-CPE elements simulating the time depending reaction in the electrode, charge transfer and mass transport respectively [32–35], enables to separate the charge transfer resistances and to compare the influence of both catalysts on the cell performance. Indeed, the cell containing $Ir_{0.7}Ru_{0.3}O_x$ (EC) shows a higher ohmic resistance, 25.8 mΩ cm², which affects the cell performance negatively, especially at high current densities. The mass transport limitations are insignificant in

both cells. Assuming that in the measured range of current density all measured impedances except of the charge transfer one are constant, it is possible to plot the charge transfer overpotentials as shown in the inset of figure 4 (a). It shows a similar parallel potential shift as the cell characteristic, evidently indicating the better intrinsic catalysis properties of $Ir_{0.7}Ru_{0.3}O_x$ (EC) compared with $Ir_{0.7}Ru_{0.3}O_2$ (TT).

Catalyst stability was evaluated by long-term electrolyzer operation test. Figure 4 (b) depicts the cell potential changes during ca. 400 h constant running under a current density of 1 A cm^{-2} at 80°C. Both cells showed considerable stability but divergent durability behaviors during measurement time. $Ir_{0.7}Ru_{0.3}O_2$ (TT) shows a constant cell potential increase, 43 µV h^{-1}, which is consistent with previous research [8,9]. Interestingly, the potential of $Ir_{0.7}Ru_{0.3}O_x$ (EC) is continuously decreasing during the test, -81 µV h^{-1}, and consequently the cell efficiency is increasing. This can be explained by two possible reasons: i) either membrane thinning due to radical attack [36]; or ii) an increase of the number of catalytically active sites. The most plausible interpretation is that the fast dissolution of Ru leads to surface roughening and thus increase in the number of active sites [16,17,37]. For a reliable conclusion on degradation effects of these materials, further investigation is required, which is ongoing. On the other hand, it is worth to mention that the dissolved Ru ions can be recovered by using ion exchange resin, which offers the possibility for Ru recycling in industry level.

In addition, from a fundamental perspective, three mechanisms have been recently proposed to explain the high OER activity of the similar Ir based catalysts: 1) Pfeifer *et al.* show the O^{I-} species formation on the amorphous IrO_x surface, which is extremely electrophilic and plays a critical role for the high OER activity by promoting O-O bond formation during OER process [38,39]; 2) Reier *et al.* prepared a series of thermally treated Ir-Ni oxides and observed an

exceptional OER activity after Ni leaching under OER condition compared to pure Ir oxide, the superior activity was attributed to the formation of reactive surface hydroxyls, which showed a reduced binding to the oxide lattice and was assumed to act as reactive surface intermediates on active sites of the catalytic process [40]; 3) a $IrO_x/IrSrO_3$ thin film derived from $IrSrO_3$ perovskite phase by strontium leaching was developed by Seitz *et al.* [20], also demonstrated an excellent OER activity in acid electrolyte, density functional theory (DFT) calculations suggest the IrO_3 or anatase IrO_2 motifs formation on the surface, which is considered to be highly active for OER [41]. In our case, the unprecedented OER activity of $Ir_{0.7}Ru_{0.3}O_x$ (EC) results from Ru leaching and the formation of an amorphous Ir oxide/hydroxide layer with low coordinates sites. Therefore, both the surface O^{I-} formation and surface hydroxyls formation are plausible explanations for a superior activity in our case and may be even descriptors of the same species. However, IrO_3 or anatase IrO_2 motifs formations are not considered as probable phase because $Ir_{0.7}Ru_{0.3}O_x$ (EC) does not appear as the perovskite phase and thermally oxidized catalyst generally yields lower activity. Further in operando measurements and fine structure spectroscopy techniques are required for validating this hypothesis.

Conclusion

In this study we report a highly active electrochemically oxidized $Ir_{0.7}Ru_{0.3}O_x$ (EC) OER catalyst for PEM electrolyzer anodes. Ru component in $Ir_{0.7}Ru_{0.3}O_x$ (EC) is highly unstable in the initial catalysis stage. However, after Ru leaching process, $Ir_{0.7}Ru_{0.3}O_x$ (EC) shows ca. 13- and 6- fold higher OER activity than $Ir_{0.7}Ru_{0.3}O_2$ (TT) and our previously reported benchmark IrO_x-Ir, respectively. The surface O^{I-} species and surface hydroxyls formation, which are highly active for catalyzing OER, are assumed to mainly contribute to the boosted OER activity [38–40]. The

durability of $Ir_{0.7}Ru_{0.3}O_x$ (EC) was tested by ca. 400 h electrolyzer measurements, showing no cell potential increasing during this time and constantly improved cell efficiency.

Acknowledgments

The authors appreciate the assistance of M. Hävecker and A. Knop-Gericke (FHI, Berlin) to this study and are indebted for the opportunity to use ISISS beamline (BESSY II). HZB (Berlin) was also been sincerely acknowledged because of synchrotron radiation beam time allocation. The research leading to these results has received funding from the European Union's Seventh Framework Program (FP7/2007-2013) for Fuel Cell and Hydrogen Joint Technology Initiative under Grant No. 621237 (INSIDE). The authors also appreciate Thierry Dintzer (ICPEES, Strasbourg) for SEM analysis, Corinne Ulhaq-Bouillet (IPCMS, Strasbourg) for TEM and STEM characterization, Anke Lützner (DLR, Stuttgart) for UHV-XPS measurements and Jörg Bürkle (DLR, Stuttgart) for his assistance on the electrolyzer stack test.

Appendix A. Supplementary material

Materials preparation, experimental details, XRD, NAP-XPS analysis and additional RDE, TEM, UHV-XPS results. Supplementary data associated with this article can be found in the online version at http://dx.doi.org/xx.xxxx/.

References

[1] M. Carmo, D.L. Fritz, J. Mergel, D. Stolten, Int. J. Hydrogen Energy 38 (2013) 4901–4934.

[2] F. Barbir, Sol. Energy 78 (2005) 661–669.

[3] E. Fabbri, A. Habereder, K. Waltar, R. Kötz, T.J. Schmidt, Catal. Sci. Technol. 4 (2014)

3800–3821.

[4] S. Park, Y. Shao, J. Liu, Y. Wang, Energy Environ. Sci. 5 (2012) 9331–9344.

[5] H. Dau, C. Limberg, T. Reier, M. Risch, S. Roggan, P. Strasser, ChemCatChem 2 (2010) 724–761.

[6] A. Di Blasi, C. D'Urso, V. Baglio, V. Antonucci, A.S. Arico', R. Ornelas, F. Matteucci, G. Orozco, D. Beltran, Y. Meas, L.G. Arriaga, J. Appl. Electrochem. 39 (2009) 191–196.

[7] Y. Lee, J. Suntivich, K.J. May, E.E. Perry, Y. Shao-Horn, J. Phys. Chem. Lett. 3 (2012) 399–404.

[8] T. Audichon, E. Mayousse, S. Morisset, C. Morais, C. Comminges, T.W. Napporn, K.B. Kokoh, Int. J. Hydrogen Energy 39 (2014) 16785–16796.

[9] S. Siracusano, N.V. Dijk, E. Payne-Johnson, V. Baglio, A.S. Aricò, Appl. Catal. B Environ. 164 (2015) 488–495.

[10] H.N. Nong, L. Gan, E. Willinger, D. Teschner, P. Strasser, Chem. Sci. 5 (2014) 2955–2963.

[11] A. Minguzzi, C. Locatelli, O. Lugaresi, E. Achilli, G. Cappelletti, M. Scavini, M. Coduri, P. Masala, B. Sacchi, A. Vertova, P. Ghigna, S. Rondinini, ACS Catal. 5 (2015) 5104–5115.

[12] R. Kötz, S. Stucki, Electrochim. Acta 31 (1986) 1311–1316.

[13] R. Kötz, S. Stucki, J. Electroanal. Chem. 172 (1984) 211–219.

[14] L. Wang, P. Lettenmeier, U. Golla-Schindler, P. Gazdzicki, N.A. Cañas, T. Morawietz, R. Hiesgen, S.S. Hosseiny, A.S. Gago, K.A. Friedrich, Phys. Chem. Chem. Phys. 18 (2016) 4487–4495.

[15] P. Lettenmeier, L. Wang, U. Golla-Schindler, P. Gazdzicki, N.A. Cañas, M. Handl, R.

Hiesgen, S.S. Hosseiny, A.S. Gago, K.A. Friedrich, Angew. Chem. 128 (2016) 752–756.

[16] N. Danilovic, R. Subbaraman, K.C. Chang, S.H. Chang, Y.J. Kang, J. Snyder, A.P. Paulikas, D. Strmcnik, Y.T. Kim, D. Myers, V.R. Stamenkovic, N.M. Markovic, J. Phys. Chem. Lett. 5 (2014) 2474–2478.

[17] N. Danilovic, R. Subbaraman, K.C. Chang, S.H. Chang, Y. Kang, J. Snyder, A.P. Paulikas, D. Strmcnik, Y.T. Kim, D. Myers, V.R. Stamenkovic, N.M. Markovic, Angew. Chem. 126 (2014) 14240–14245.

[18] J.Y. Kim, J. Choi, H.Y. Kim, E. Hwang, H.J. Kim, S.H. Ahn, S.K. Kim, Appl. Surf. Sci. 359 (2015) 227–235.

[19] S. Cherevko, T. Reier, A.R. Zeradjanin, Z. Pawolek, P. Strasser, K.J.J. Mayrhofer, Electrochem. Commun. 48 (2014) 81–85.

[20] L.C. Seitz, C.F. Dickens, K. Nishio, Y. Hikita, J. Montoya, A. Doyle, C. Kirk, A. Vojvodic, H.Y. Hwang, J.K. Norskov, T.F. Jaramillo, Science 353 (2016) 1011–1014.

[21] V.A. Saveleva, L. Wang, W. Luo, S. Zafeiratos, C. Ulhaq-Bouillet, A.S. Gago, K.A. Friedrich, E.R. Savinova, J. Phys. Chem. Lett. 2 (2016) 3240–3245.

[22] J. Cheng, H. Zhang, G. Chen, Y. Zhang, Electrochim. Acta 54 (2009) 6250–6256.

[23] A.T. Marshall, R.G. Haverkamp, Electrochim. Acta 55 (2010) 1978–1984.

[24] C. Angelinetta, S. Trasatti, L.D. Atanososka, R.T. Atanasoski, J. Electroanal. Chem. 214 (1986) 535–546.

[25] R. Hutchings, K. Müller, R. Kötz, S. Stucki, J. Mater. Sci. 19 (1984) 3987–3994.

[26] S.M. Lin, T.C. Wen, J. Electrochem. Soc. 140 (1993) 2265–2271.

[27] L.E. Owe, M. Tsypkin, K.S. Wallwork, R.G. Haverkamp, S. Sunde, Electrochim. Acta 70 (2012) 158–164.

[28] S. Cherevko, A.R. Zeradjanin, A.A. Topalov, N. Kulyk, I. Katsounaros, K.J.J. Mayrhofer, ChemCatChem 6 (2014) 2219–2223.

[29] T. Reier, M. Oezaslan, P. Strasser, ACS Catal. 2 (2012) 1765–1772.

[30] H.S. Oh, H.N. Nong, T. Reier, M. Gliech, P. Strasser, Chem. Sci. 6 (2015) 3321–3328.

[31] H. Over, Chem. Rev. 112 (2012) 3356–3426.

[32] J.T. Mueller, P.M. Urban, J. Power Sources 75 (1998) 139–143.

[33] O. Antoine, Y. Bultel, R. Durand, J. Electroanal. Chem. 499 (2001) 85–94.

[34] M. Eikerling, A.A. Kornyshev, J. Electroanal. Chem. 475 (1999) 107–123.

[35] P. Lettenmeier, S. Kolb, F. Burggraf, A.S. Gago, K.A. Friedrich, J. Power Sources 311 (2016) 153–158.

[36] S. Stucki, G.G. Scherer, S. Schlagowski, E. Fischer, J. Appl. Electrochem. 28 (1998) 1041–1049.

[37] S. Cherevko, S. Geiger, O. Kasian, N. Kulyk, J. Grote, A. Savan, B.R. Shrestha, S. Merzlikin, B. Breitbach, A. Ludwig, K.J.J. Mayrhofer, Catal. Today 262 (2016) 170–180.

[38] V. Pfeifer, T.E. Jones, S. Wrabetz, C. Massué, J.J. Velasco Vélez, R. Arrigo, M. Scherzer, S. Piccinin, M. Hävecker, A. Knop-Gericke, R. Schlögl, Chem. Sci. 7 (2016) 6791–6795.

[39] V. Pfeifer, T.E. Jones, J.J. Velasco Vélez, R. Arrigo, S. Piccinin, M. Hävecker, A. Knop-Gericke, R. Schlögl, Chem. Sci. (2017). In press, DOI:10.1039/C6SC04622C.

[40] T. Reier, Z. Pawolek, S. Cherevko, M. Bruns, T. Jones, D. Teschner, S. Selve, A. Bergmann, H.N. Nong, R. Schlögl, K.J.J. Mayrhofer, P. Strasser, J. Am. Chem. Soc. 137 (2015) 13031–13040.

[41] Z. Xu, J.R. Kitchin, Phys. Chem. Chem. Phys. 17 (2015) 28943–28949.

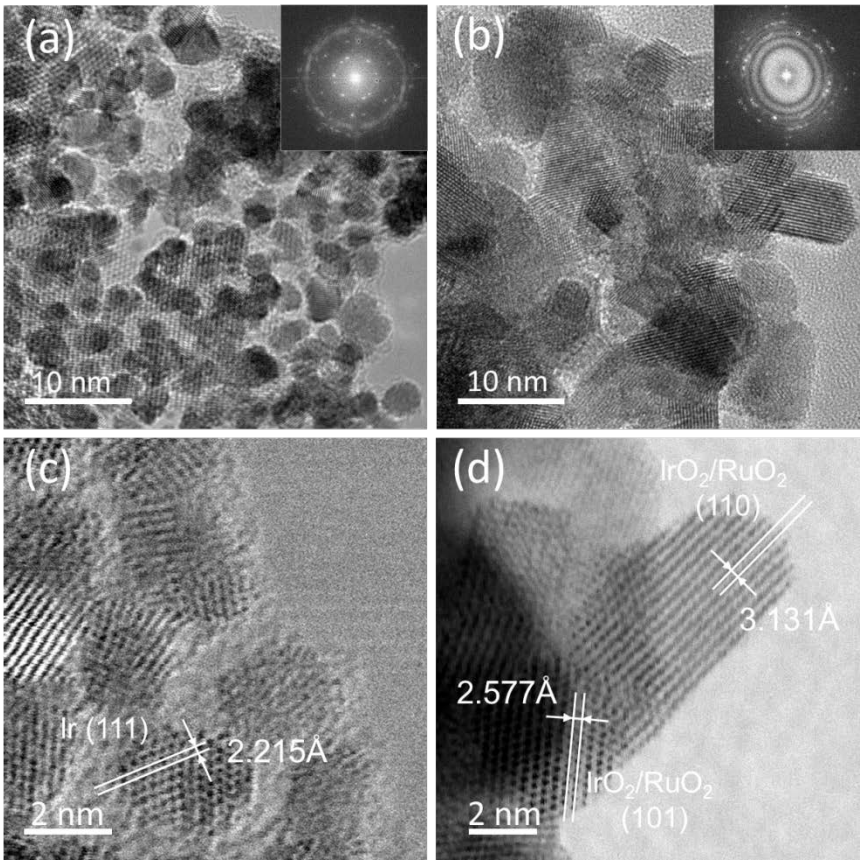

Figure 1 TEM (upper panels) and STEM (bottom panels) images of $Ir_{0.7}Ru_{0.3}$-pristine (a,c) and $Ir_{0.7}Ru_{0.3}O_2$ (TT) (b,d), insets of panel (a) and (b) are FFT of the selected area of corresponding catalyst particles.

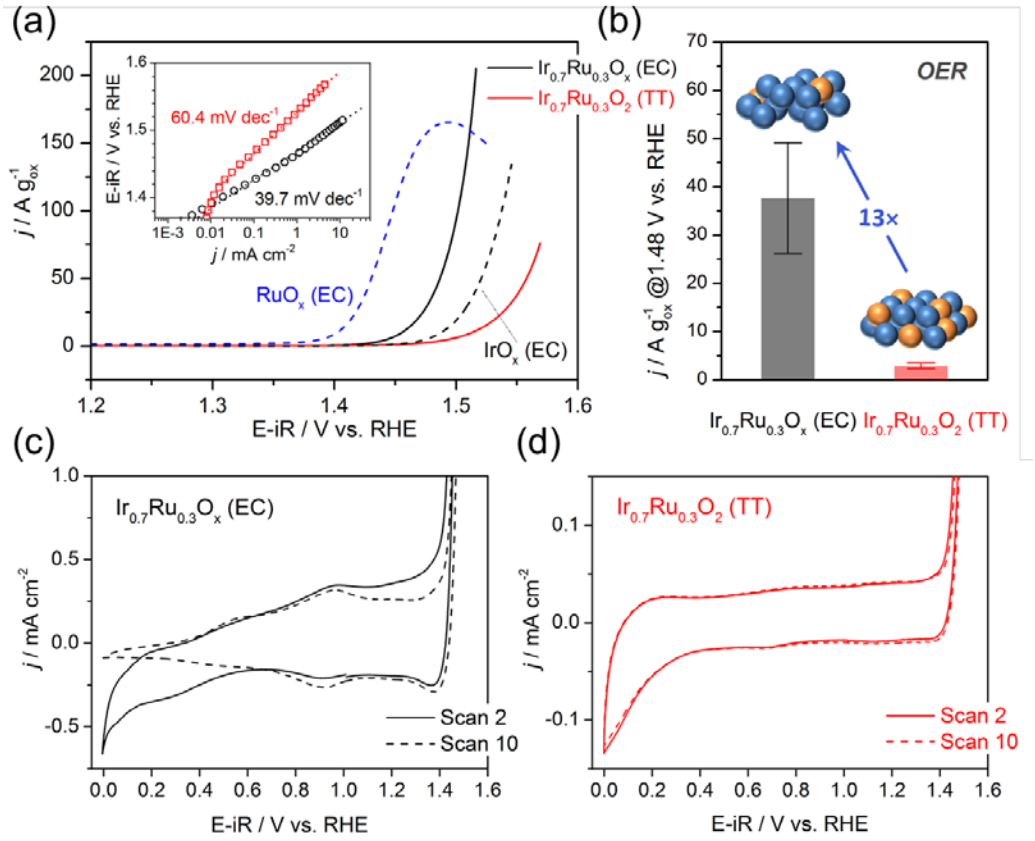

Figure 2 (a) Oxygen evolution reaction (OER) activities comparison among $Ir_{0.7}Ru_{0.3}O_x$ (EC), IrO_x (EC) and $Ir_{0.7}Ru_{0.3}O_2$ (TT) after EC protocol, blue dashed line showed the initial OER activity of RuO_x (EC) out of CV cycle 2 (inset: tafel slope of $Ir_{0.7}Ru_{0.3}O_x$ (EC) and $Ir_{0.7}Ru_{0.3}O_2$ (TT)), N_2-saturated 0.05 M H_2SO_4, 25 °C, rotating rate: 1600 rpm, scanning rate: 5 mV s^{-1}; (b) Mass activity comparison with an overpotential of 250 mV between $Ir_{0.7}Ru_{0.3}O_x$ (EC) and $Ir_{0.7}Ru_{0.3}O_2$ (TT); (c) Cyclic voltammetry curves of (c) $Ir_{0.7}Ru_{0.3}O_x$ (EC) sample and (d) $Ir_{0.7}Ru_{0.3}O_2$ (TT) sample between cycle 2 and cycle 10, scanning rate: 20 mV s^{-1}.

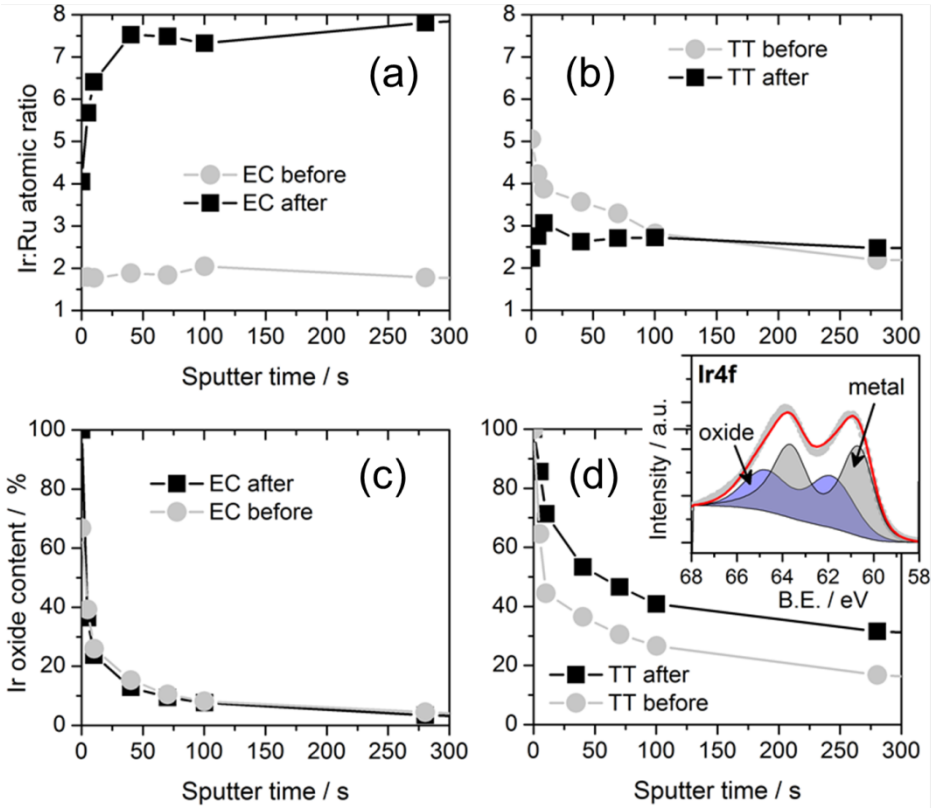

Figure 3 *ex situ* XPS analysis of $Ir_{0.7}Ru_{0.3}O_x$ (EC) and $Ir_{0.7}Ru_{0.3}O_2$ (TT) anodes before and after electrolysis operation for 18h at 1.6 V: Ir/Ru atomic ration versus sputter time of the sample EC (a) and TT (b); (b) Ir/Ru atomic ration versus sputter time of the TT sample; Ir-oxide content relative to overall Ir versus sputter time for the sample EC (c) and TT (d). The inset of (d) shows fitted Ir metal and oxide XPS peaks (B.E.=Binding Energy) used for the quantification of Ir-oxide in (c) and (d).

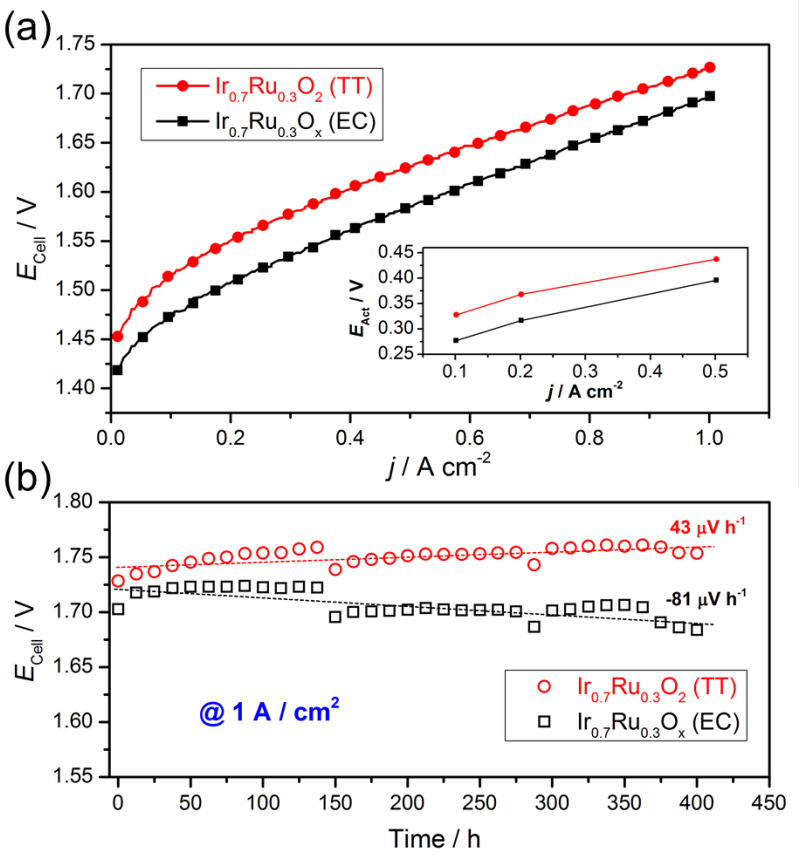

Figure 4 (a) 25 cm^2 PEM electrolyzer tests in a 2-cell stack having MEAs with $Ir_{0.7}Ru_{0.3}O_x$ (EC) and $Ir_{0.7}Ru_{0.3}O_2$ (TT) anodes, 1 mg of powder cm^{-2}. Cathode catalyst, 40 wt.% Pt/C, 0.4 mg Pt cm^{-2}; Nafion®212; 1 bar, 80 °C; (b) 400 hour durability test under a constant current density of 1 A cm^{-2}; inset of panel (a) shows the overpotentials only representing the charge transfer for EC and TT.

Graphical Abstract